JACS
JOURNAL OF THE AMERICAN CHEMICAL SOCIETY
Article
Cite This: J. Am. Chem. Soc. 2018, 140, 11133−11140
pubs.acs.org/JACS

Efficient Removal of $[UO_2]^{2+}$, Cs^+, and Sr^{2+} Ions by Radiation-Resistant Gallium Thioantimonates

Mei-Ling Feng,[†,‡] Debajit Sarma,[‡] Yu-Jie Gao,[†,§] Xing-Hui Qi,[†,§] Wei-An Li,[†,§] Xiao-Ying Huang,*[,†] and Mercouri G. Kanatzidis*[,‡]

[†]State Key Laboratory of Structural Chemistry, Fujian Institute of Research on the Structure of Matter, Chinese Academy of Sciences, Fuzhou, Fujian 350002, People's Republic of China

[‡]Department of Chemistry, Northwestern University, 2145 Sheridan Road, Evanston, Illinois 60208, United States

[§]College of Chemistry, Fuzhou University, Fuzhou, Fujian 350002, People's Republic of China

Supporting Information

ABSTRACT: Unconventional ion exchangers can achieve efficient removal of $[UO_2]^{2+}$, Cs^+, and Sr^{2+} ions from complex aqueous solutions and are of great interest for environmental remediation. We report two new gallium thioantimonates, $[Me_2NH_2]_2[Ga_2Sb_2S_7]\cdot H_2O$ (FJSM-GAS-1) and $[Et_2NH_2]_2[Ga_2Sb_2S_7]\cdot H_2O$ (FJSM-GAS-2), which present excellent ion exchange properties for $[UO_2]^{2+}$, Cs^+, and Sr^{2+} ions. They exhibit high ion exchange capacities for $[UO_2]^{2+}$, Cs^+, and Sr^{2+} ions (q_m^U = 196 mg/g, q_m^{Cs} = 164 mg/g, and q_m^{Sr} = 80 mg/g for FJSM-GAS-1, q_m^U = 144 mg/g for FJSM-GAS-2) and short equilibrium times for $[UO_2]^{2+}$ ion exchange (5 min for FJSM-GAS-1 and 15 min for FJSM-GAS-2, respectively). Both compounds display active ion exchange with $[UO_2]^{2+}$ in the pH range of 2.9−10.5. Moreover, the sulfide compounds could maintain high distribution coefficients K_d^U even in the presence of excess Na^+, Ca^{2+}, and HCO_3^-. The distribution coefficient K_d^U of 6.06×10^6 mL/g exhibited by FJSM-GAS-1 is the highest among the reported U adsorbents. The $[UO_2]^{2+}$-laden products can be recycled by conveniently eluting the uranium with a low-cost method. These advantages combined with facile synthesis, as well as β and γ radiation resistance, make FJSM-GAS-1 and FJSM-GAS-2 promising for selective separations in nuclear waste remediation.

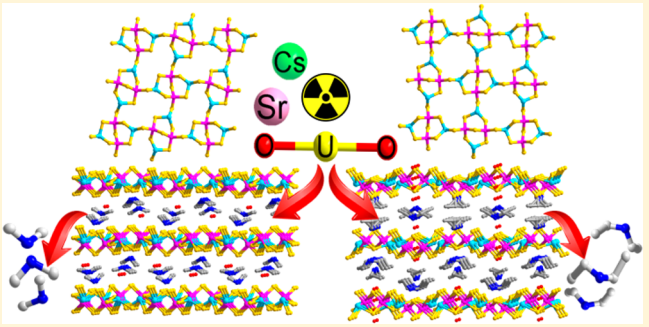

INTRODUCTION

Although nuclear power provides efficient, cheap, and sustainable energy for the world's electricity production, environmental concerns associated with the nuclear fuel cycle persist, such as the efficient handling of nuclear waste and reactor accidents.[1] Nuclear waste solutions contain a variety of dilute radioactive ions mixed with more concentrated conventional ions such as Na^+. Uranium is an essential element with radioactivity and high chemical toxicity in the nuclear fuel cycle. Uranyl cations $[UO_2]^{2+}$ can dissolve in water and cause environmental and human health problems.[2] Uranium harvesting is also of interest in nuclear energy generation. About 4.5 billion tons of uranium (about 3.3 ppb) is present in the ocean, and it is very appealing to find ways to capture it.[3] In addition to uranium, $^{137}Cs^+$ and $^{90}Sr^{2+}$ ions are the main hazardous byproducts in nuclear waste. They produce γ and high-energy β particles with long half-lives (a half-time of $t_{1/2} \approx 30$ years for ^{137}Cs and $t_{1/2} \approx 29$ years for ^{90}Sr).[4] Therefore, it is vitally important to efficiently remove and recover radioactive $[UO_2]^{2+}$, Cs^+, and Sr^{2+} ions for the sake of human health, environmental protection, and energy recycling.

There is a large excess of nonradioactive Na^+ and Ca^{2+} ions in nuclear waste solutions, which have a huge impact on the selective uptake of $[UO_2]^{2+}$, Cs^+, and Sr^{2+} ions. To remove these radionuclides, many techniques and versatile materials have been explored such as membrane filtration, solvent extraction, adsorption, and ion exchange.[5] The ion exchange method can deliver high selectivity, minimal radioactive discharge, and solidified waste.[5a,6] Organic-based ion exchange materials have some disadvantages in nuclear waste disposal, such as stability problems and relatively high cost, while inorganic oxide ion exchangers often suffer from low selectivity and a narrow pH range of application.[7] Therefore, it is important to develop new ion exchangers for efficient and selective capture of $[UO_2]^{2+}$, Cs^+, and Sr^{2+} ions from complex aqueous solutions.

Compared with the oxides, metal chalcogenides possess more flexible networks and soft Lewis basic sites of Q^{2-} (Q = S and Se) that have an innate affinity toward soft metal ions in the process of ion exchange.[5a,8] Open-framework metal

Received: July 15, 2018
Published: August 8, 2018

DOI: 10.1021/jacs.8b07457
J. Am. Chem. Soc. 2018, 140, 11133−11140

chalcogenides as ion exchangers have exhibited high ion exchange capacity and excellent selectivity for metal ions Cs^+, Sr^{2+}, Pb^{2+}, Hg^{2+}, and Cd^{2+} against hard ions such as Na^+ and Ca^{2+}.[5a,9] It has also been proved that the $[UO_2]^{2+}$ ion can be captured by metal chalcogenides via strong $[UO_2]^{2+}\cdots S^{2-}$ bonding interactions despite the fact that $[UO_2]^{2+}$ is widely regarded as a hard Lewis acid.[10] So far, a few inorganic chalcogenide capturers for radioactive $[UO_2]^{2+}$, Cs^+, Sr^{2+} ions, etc., have been reported, such as $K_{2x}Mn_xSn_{3-x}S_6$ (x = 0.5−0.95, KMS-1),[9i,k,10c] $K_{2x}Mg_xSn_{3-x}S_6$ (x = 0.5−1, KMS-2),[9h] $KInSn_2S_6$ (KMS-5),[11] $K_{2x}Sn_{4-x}S_{8-x}$ (x = 0.65−1, KTS-3),[9a,b] $K_6Sn[Zn_4Sn_4S_{17}]$,[12] $K_{14-x}H_xCd_{15}Sn_{12}Se_{46}$ ($x \approx 7$)[13] and polysulfide/layered double hydroxide composites (S_x-LDH, x = 2, 4).[10b] In addition, several hybrid organic−inorganic chalcogenide ion exchange materials have been reported such as $(Me_2NH_2)_{1.33}(Me_3NH)_{0.67}Sn_3S_7\cdot 1.25H_2O$ (FJSM-SnS),[9d,10a,14] $[(Me)_2NH_2]_2[GeSb_2S_6]$,[9j] $[(Me)_2NH_2]_{0.75}[Ag_{1.25}SnSe_3]$,[15] $[CH_3NH_3]_4[In_4SbS_9SH]$,[16] and $[CH_3NH_3]_{20}Ge_{10}Sb_{28}S_{72}\cdot 7H_2O$.[9c] In particular, the layered microporous FJSM-SnS exhibits outstanding ion exchange properties for $[UO_2]^{2+}$, Cs^+, and Sr^{2+} ions and the recovery of rare earth elements.[14] The protonated organic amines have the advantage of conformational flexibility, size tunability, and structural diversity.

Herein, we present two new gallium thioantimonates, namely, $[Me_2NH_2]_2[Ga_2Sb_2S_7]\cdot H_2O$ (FJSM-GAS-1) and $[Et_2NH_2]_2[Ga_2Sb_2S_7]\cdot H_2O$ (FJSM-GAS-2). Both compounds are easily prepared by a straightforward, one-pot, solvothermal method. We show here that they exhibit excellent β and γ radiation resistance, which has been rarely studied in metal sulfide ion exchange materials. Their ion exchange properties for $[UO_2]^{2+}$, Cs^+, and Sr^{2+} ions have been systematically studied. The equilibrium model studies show that FJSM-GAS-1 and FJSM-GAS-2 have high ion exchange capacities for $[UO_2]^{2+}$, Cs^+, and Sr^{2+} ions (q_m^U = 196 mg/g, q_m^{Cs} = 164 mg/g, and q_m^{Sr} = 80 mg/g for FJSM-GAS-1; q_m^U = 144 mg/g for FJSM-GAS-2). Our kinetic studies show a short equilibrium time for $[UO_2]^{2+}$ ion exchange (5 min for FJSM-GAS-1 and 15 min for FJSM-GAS-2, respectively). Both compounds are active for $[UO_2]^{2+}$ in the pH range of 2.9−10.5 and exhibit excellent selectivity. Particularly, the distribution coefficient K_d^U of 6.06×10^6 mL/g for FJSM-GAS-1 is the highest among all reported U adsorbents even in the presence of a large excess of Na^+. The $[UO_2]^{2+}$-laden products could be conveniently recycled by eluting the uranium with potassium chloride solution, further highlighting the value of current compounds for radionuclide remediation.

EXPERIMENTAL SECTION

Materials and Synthesis. $Ga(NO_3)_3\cdot 9H_2O$ (99.99%, Shanghai Longjin Metallic Material Co., Ltd.), $Sb(CH_3COO)_3$ (97%, Aladdin), sulfur powder (CP, Sinopharm Chemical Reagent Co., Ltd.), methanol (AR, Sinopharm Chemical Reagent Co., Ltd.), dimethylamine aqueous solution (33%, CP, Sinopharm Chemical Reagent Co., Ltd.), and diethylamine (AR, Sinopharm Chemical Reagent Co., Ltd.) were used without further purification.

Solvothermal Synthesis of FJSM-GAS-1. FJSM-GAS-1 was synthesized by heating a mixture of $Ga(NO_3)_3\cdot 9H_2O$ (0.52 mmol, 0.216 g), $Sb(CH_3COO)_3$ (0.49 mmol, 0.147 g), S (4.69 mmol, 0.150 g), 2 mL of dimethylamine aqueous solution (33%), and 2 mL of methanol in a 20 mL stainless steel reactor with a Teflon liner at 160 °C for 6 days. Larger-scale synthesis of FJSM-GAS-1: A mixture of $Ga(NO_3)_3\cdot 9H_2O$ (4.71 mmol, 1.970 g), $Sb(CH_3COO)_3$ (4.79 mmol, 1.433 g), and S (39.75 mmol, 1.272 g) in 20 mL of dimethylamine aqueous solution (33%) and 20 mL of methanol was stirred under ambient conditions until homogeneous. The resulting mixture sealed in a 235 mL stainless steel reactor with a Teflon liner was heated at 160 °C for 6 days and then cooled to room temperature. Yellow, brick-like crystals were obtained by filtration. The crystalline products were washed by water and ethanol and air-dried (yield: 1.491 g, 88% based on Ga). Anal. Calcd for $C_4H_{18}N_2Ga_2Sb_2S_7O$: C, 6.70%; H, 2.53%; N, 3.90%; S, 31.28%. Found: C, 6.75%; H, 2.41%; N, 3.91%; S, 31.21%.

Solvothermal Synthesis of FJSM-GAS-2. FJSM-GAS-2 was synthesized by heating a mixture of $Ga(NO_3)_3\cdot 9H_2O$ (0.47 mmol, 0.195 g), $Sb(CH_3COO)_3$ (0.49 mmol, 0.146 g), S (4.90 mmol, 0.157 g), 2 mL of diethylamine, and 2 mL of methanol in a 20 mL stainless steel reactor with a Teflon liner at 160 °C for 6 days. Larger-scale synthesis of FJSM-GAS-2: A mixture of $Ga(NO_3)_3\cdot 9H_2O$ (4.89 mmol, 2.043 g), $Sb(CH_3COO)_3$ (4.93 mmol, 1.475 g), and S (48.94 mmol, 1.566 g) in 20 mL of diethylamine and 20 mL of methanol was stirred under ambient conditions until homogeneous. The resulting mixture sealed in a 235 mL stainless steel reactor with a Teflon liner was heated at 160 °C for 6 days and then cooled to room temperature. Yellow, brick-like crystals were obtained by filtration. The crystalline products were washed by water and ethanol and air-dried (yield: 1.342 g, 71% based on Ga). Anal. Calcd for $C_8H_{26}N_2Ga_2Sb_2S_7O$: C, 12.42%; H, 3.39%; N, 3.62%; S, 29.01%. Found: C, 13.01%; H, 3.22%; N, 3.66%; S, 29.47%.

Soaking Experiments of Materials Before and After Irradiation. In the soaking experiments, 10 mg of FJSM-GAS-1 and FJSM-GAS-2 and their samples after 100 and 200 kGy β irradiation and 200 kGy γ irradiation were dispersed in 10 mL of water, respectively. Then the concentrations of leaching Ga, Sb, and S ions were checked (Table S3).

Ion Exchange Experiments. A representative ion exchange experiment was performed in an aqueous solution of $UO_2(NO_3)_2\cdot 6H_2O$, CsCl, or $SrCl_2$, respectively, in which the ground polycrystalline powder of FJSM-GAS-1 or FJSM-GAS-2 was added. The mixture was held under magnetic stirring for 24 h at room temperature. Then the ion-exchanged FJSM-GAS-1 or FJSM-GAS-2 was separated by centrifugation and filtration (through filter paper, Whatman no. 1) and washed several times with deionized water. The concentrations of $[UO_2]^{2+}$, Cs^+, and Sr^{2+} in the filtered solution were determined by inductively coupled plasma atomic emission spectroscopy (ICP-OES) and inductively coupled plasma mass spectroscopy (ICP-MS).

In isotherm experiments, solutions of Cs^+ (167−1276 ppm) and Sr^{2+} (36−901 ppm) with different concentrations were prepared, respectively. The initial solutions with various concentrations of uranium (13−1011 ppm) were prepared whose pH values were adjusted using NaOH solution to the range of 4 to 7 in order to avoid hydrolysis and the superacidic condition of an aqueous solution of $UO_2(NO_3)_2\cdot 6H_2O$. The isotherm experiments were done by the batch method at a V/m ratio of 1000 mL/g (V = 10 mL, m = 10 mg), room temperature, and 24 h contact time. In kinetics experiments of $[UO_2]^{2+}$ ion exchange, the initial concentration of uranium was 1348 ppb and the V:m was 1000 mL/g (V = 20 mL, m = 20 mg) at room temperature. The kinetics experiments of various reaction times (5, 15, 30, 65, 180, 300, and 1740 min) were carried out (Table S4). Then all the samples were taken out and processed.

In pH-dependent experiments of $[UO_2]^{2+}$ ion exchange for FJSM-GAS-1 and FJSM-GAS-2, the $[UO_2]^{2+}$ solutions in the pH range of 2.9 to 10.5 were prepared (Tables S6 and S7). The pH values of $[UO_2]^{2+}$ solutions with initial concentrations of uranium from 1468 to 2436 ppb were controlled by diluting a HCl or NaOH solution. V/m was 1000 mL/g at room temperature and 24 h contact time. The selective $[UO_2]^{2+}$-exchanged experiments with excess $NaNO_3$, NaCl, $NaHCO_3$, and $CaCl_2$ were performed at V/m ratios of 1000 or 200 mL/g, 24 h contact time, and room temperature (Tables S8 and S9).

The $[UO_2]^{2+}$-exchanged products from the exchange capacity experiments that had an initial 1011 ppm uranium were used in the elution experiments. Both $[UO_2]^{2+}$-exchanged products of FJSM-GAS-1 (~5 mg) and FJSM-GAS-2 (~5 mg) were soaked in 10 mL of concentrated KCl solution (0.2 M) under magnetic stirring for 24 h at

DOI: 10.1021/jacs.8b07457
J. Am. Chem. Soc. 2018, 140, 11133−11140

room temperature. Then the solid products were separated from the solution and checked with powder X-ray diffraction (PXRD) and energy dispersive spectroscopy (EDS).

Characterization Techniques. ThermoFisher iCapQ ICP-MS and ThermoFisher iCap7600 ICP-OES instruments were applied for the analyses of concentrations of metal ions in the solution. Elemental analyses of C, H, N, and S were carried out on a German Elementary Vario EL III instrument. EDS and scanning electron spectroscopy (SEM) analyses were done on a Hitachi S-3400N-II scanning electron microscope with an ESED II detector. The elemental analyses of the metal were performed with an accelerating voltage of 20 kV and 60 s acquisition time. PXRD patterns were finished with a CPS 120 INEL X-ray powder diffractometer with graphite-monochromated Cu Kα radiation operating at 40 kV and 20 mA at room temperature. Infrared spectra were obtained with a Bruker Tensor 37 FTIR (MID IR/ATR) using an attenuated total reflectance attachment in the range 4000–400 cm^{-1}. X-ray photoelectron spectra (XPS) were collected by applying a Thermo Scientific ESCALAB 250 Xi spectrometer equipped with a monochromatic Al Kα X-ray source (1486.6 eV) performing at 300 W.

Both compounds were irradiated at a dose rate of 1.2 kGy/h for three different doses of 20, 100, and 200 kGy in the ^{60}Co γ irradiation experiment and at a dose rate of 20 kGy/h for two different doses of 100 and 200 kGy in the β irradiation experiment, respectively. β irradiation was conducted using electron beams (10 MeV) that were provided by an electron accelerator located in CGN Dasheng Electron Accelerator Co., Ltd., in Jiangsu Province, China. The single-crystal X-ray diffraction data for FJSM-GAS-1 and FJSM-GAS-2 were collected on an Oxford Xcalibur Eos CCD diffractometer with graphite-monochromated Mo Kα (0.710 73 Å) at room temperature. The structures were solved by direct methods and refined by full-matrix least-squares on F^2 by using the program SHELX-2016.[17] CCDC 1580659 and CCDC 1580660 are for FJSM-GAS-1 and FJSM-GAS-2, respectively.

RESULTS AND DISCUSSION

Crystal Structures. The yellow, brick-like crystals of FJSM-GAS-1 and FJSM-GAS-2 are stable in air (Figure 1a and b). Both compounds represent two new gallium thioantimonates containing protonated organic amine cations, and their structures feature the inorganic anionic two-dimensional (2D) networks built upon Ga/Sb tetranuclear heterometallic units with organic amine cations located at the interlayer spaces. Single-crystal X-ray analyses reveal that FJSM-GAS-1 and FJSM-GAS-2 crystallize in the space group $P2_12_12_1$ and $I4_1/a$, respectively (Table S1). The general formula of both compounds is $(R_2NH_2)_2[Ga_2Sb_2S_7]\cdot H_2O$, and they are part of a broader family of gallium thioantimonate analogues.[9e,18] The asymmetric unit of FJSM-GAS-1 contains two crystallographically independent Ga^{3+} ions, two Sb^{3+} ions, seven S^{2-} ions, two $[Me_2NH_2]^+$ cations, and one lattice water molecule (Figure S1). The asymmetric unit of FJSM-GAS-2 contains one crystallographically independent Ga^{3+} ion, one Sb^{3+} ion, three and a half S^{2-} ions, two half-$[Et_2NH_2]^+$ cations, and two quarter lattice water molecules (Figure S2).

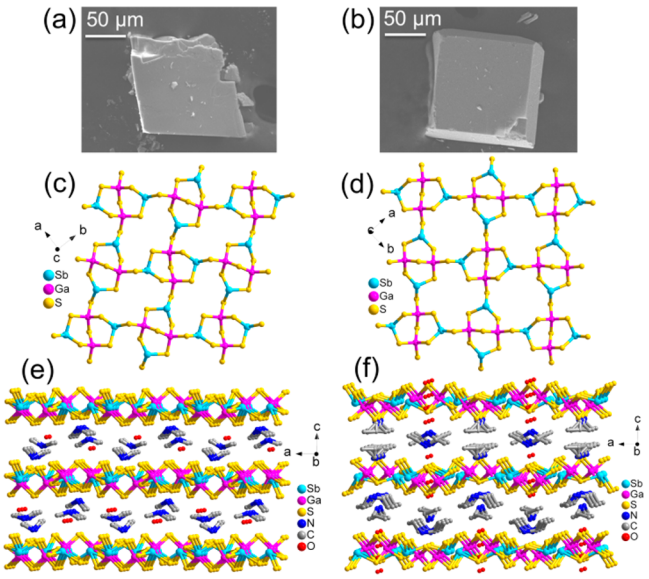

Figure 1. SEM images of an FJSM-GAS-1 (a) and an FJSM-GAS-2 crystal (b). 2D grid-like layers of $[Ga_2Sb_2S_7]_n^{2n-}$ along the *ab* plane in FJSM-GAS-1 (c) and FJSM-GAS-2 (d). Packings of layers in FJSM-GAS-1 (e) and FJSM-GAS-2 (f) in a perspective view along the *b*-axis, and the hydrogen atoms are omitted for clarity.

The structure of both layered inorganic frameworks is similar to that of $[(CH_3)_2NH_2]_2[Ga_2Sb_2S_7]\cdot H_2O$ (space group $P2_1$) with the diffrence being in the conformations of the layers that are affected by the interactions between layers and the organic cations.[18] In both compounds, the Ga^{3+} ions are tetrahedrally coordinated by four S^{2-} ions, while the Sb^{3+} ions all adopt $[SbS_3]$ trigonal pyramidal coordination geometries with Sb–S bond lengths ranging from 2.411(3) to 2.437(4) Å. Each S^{2-} anion acts as a bidentate metal linker. The Ga/Sb tetranuclear heterometallic unit with a stoichiometry of $[Ga_2Sb_2S_9]$ is formed with two $[GaS_4]$ tetrahedra and two $[SbS_3]$ trigonal pyramids interconnected by corner-sharing. The $[Ga_2Sb_2S_9]$ units are then joined by S^{2-} linkers, resulting in a grid-like layer of $[Ga_2Sb_2S_7]_n^{2n-}$ with eight-membered rings along the *ab* plane, but the grid-like layer of FJSM-GAS-2 is different than that in FJSM-GAS-1. In FJSM-GAS-2, the eight-membered rings present two kinds of squares with respective diagonal Ga···Ga distances of 9.4223(2) and 9.6712(2) Å (Figure 1d). Then the adjacent grid-like layers are stacked in *AA* sequence along the *c*-axis in both compounds (Figure 1e and f). The lone-pair electrons of Sb^{3+} are oriented toward the interlayer spaces. $[Me_2NH_2]^+$ and $[Et_2NH_2]^+$ cations as structure directing agents and charge-balancing agents are located at the interlayer spaces of FJSM-GAS-1 and FJSM-GAS-2, respectively. The lattice water molecules lie in the interlayer spaces in FJSM-GAS-1 and FJSM-GAS-2, while in FJSM-GAS-2 some of them also hide in the layers themselves. Although several gallium thioantimonates with similar grid-like layers of $[Ga_2Sb_2S_7]_n^{2n-}$ have been reported,[9e,18] their space groups are different. The comparison between reported gallium thioantimonates and the title compounds is listed in Table S2. Note that FJSM-GAS-2 presents a square grid-like layer of $[Ga_2Sb_2S_7]_n^{2n-}$ that is conformationally different from the oval grid-like layers of FJSM-GAS-1 and other reported gallium thioantimonates.[9e,18]

FJSM-GAS-1 and FJSM-GAS-2 for $[UO_2]^{2+}$, Cs^+, and Sr^{2+} Ion Exchange. PXRDs of both FJSM-GAS-1 and FJSM-GAS-2 samples after β and γ irradiation indicate no structural and crystal degradation even under 100 and 200 kGy β irradiation (10 MeV) or 200 kGy ^{60}Co γ irradiation (Figure 2). Moreover, soaking experiments done after β and γ irradiation in water suggest no leaching of Ga, Sb, and S ions, indicating irradiation has no measurable effect on the materials (Table S3). These results indicate that FJSM-GAS-1 and FJSM-GAS-2 possess the necessary radiolytic stability for the removal of radionuclides.

DOI: 10.1021/jacs.8b07457
J. Am. Chem. Soc. 2018, 140, 11133–11140

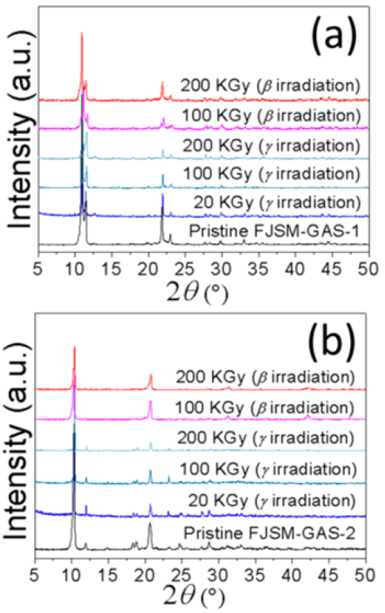

Figure 2. PXRD patterns of pristine FJSM-GAS-1 (a), FJSM-GAS-2 (b), and their corresponding samples after β and γ irradiation.

The exchange of the organic amine cations in FJSM-GAS-1 by $[UO_2]^{2+}$, Cs^+, and Sr^{2+} and FJSM-GAS-2 by $[UO_2]^{2+}$ was confirmed by EDS, XPS, ICP-OES, and ICP-MS. The EDS analyses of the products after ion exchange showed that $[UO_2]^{2+}$, Cs^+, and Sr^{2+} entered FJSM-GAS-1 and $[UO_2]^{2+}$ entered FJSM-GAS-2 (Figures S3–S6). Elemental distribution mapping of the exchanged products showed the presence of a significant amount of uranium, cesium, and strontium for FJSM-GAS-1 and uranium for FJSM-GAS-2 and their homogeneous distributions in the samples (Figures 3 and S7). The PXRD patterns of the ion-exchanged products show isotactic ion exchange with retention of the parent structure (Figure S8).

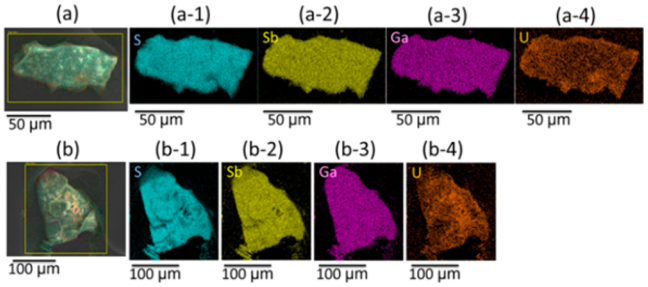

Figure 3. SEM image (a) of $[UO_2]^{2+}$-exchanged product of FJSM-GAS-1 and its elemental distribution maps of S (a-1), Sb (a-2), Ga (a-3), and U (a-4) and SEM image (b) of $[UO_2]^{2+}$-exchanged product of FJSM-GAS-2 and its elemental distribution maps of S (b-1), Sb (b-2), Ga (b-3), and U (b-4).

In contrast with the infrared spectra of the pristine compounds, those of uranyl-exchanged FJSM-GAS-1 and FJSM-GAS-2 products display the characteristic peaks of the antisymmetric vibration of $[O{=}U{=}O]^{2+}$ group at 919 and 917 cm^{-1}, respectively, which have evident red shifts compared with the peaks for aqueous $[O{=}U{=}O]^{2+}$ ions (963 cm^{-1}) (Figure S9).[19]

Adsorption Isotherm Studies of $[UO_2]^{2+}$, Cs^+, and Sr^{2+} Ion Exchange. In order to evaluate the ion exchange capacity of FJSM-GAS-1 and FJSM-GAS-2, isotherm equilibrium experiments were carried out at room temperature. The $[UO_2]^{2+}$ equilibrium curves for FJSM-GAS-1 and FJSM-GAS-2 and the Cs^+ and Sr^{2+} equilibrium curves for FJSM-GAS-1 are shown in Figure 4, which are derived from U, Cs, and Sr

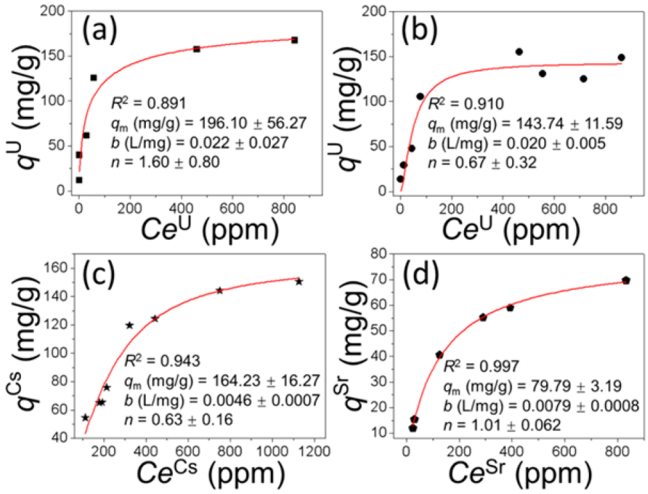

Figure 4. Equilibrium data for $[UO_2]^{2+}$ ion exchange of FJSM-GAS-1 (a) and FJSM-GAS-2 (b). Equilibrium data for Cs^+ (c) and Sr^{2+} (d) ion exchange of FJSM-GAS-1. The solid red lines are the fitting of the data with the Langmuir–Freundlich isotherm model, respectively.

concentration C_e (ppm) at equilibrium plotted against the ion exchange capacity q (mg/g) of U, Cs, and Sr. The value of q, the amount of cation exchanged at equilibrium concentration C_e (ppm), can be obtained from eq 1. C_0 is the initial concentration of the ions. V is the volume (mL) of the testing solution, and m is the mass of the ion exchanger (g). The equilibrium data for the ions were fitted with the Langmuir–Freundlich adsorption isotherms depicted by eq 2, in which b (L/mg) is a constant related to the free energy of ion exchange, n is also a constant, and q_m is the maximum ion exchange capacity (mg/g).[20]

$$q = \frac{(C_0 - C_e)V}{m} \quad (1)$$

$$q = q_m \frac{(bC_e)^{1/n}}{1 + (bC_e)^{1/n}} \quad (2)$$

From the Langmuir–Freundlich isotherm models the maximum ion exchange capacities (q_m) were found to be 196 ± 56 mg/g for uranium of FJSM-GAS-1, 144 ± 12 mg/g for uranium of FJSM-GAS-2, 164 ± 16 mg/g for cesium of FJSM-GAS-1, and 80 ± 3 mg/g for strontium of FJSM-GAS-1, respectively, Figure 4. Assuming all the organic amine cations are exchanged, the theoretical ion exchange capacities for FJSM-GAS-1 are 332 mg/g for uranium, 370 mg/g for cesium, and 122 mg/g for strontium, and that for FJSM-GAS-2 is 308 mg/g for uranium. The observed ion exchange capacities of FJSM-GAS-1 are 59% for uranium, 44% for cesium, and 65% for strontium of the theoretical ones, respectively, while that of FJSM-GAS-2 for uranium is 47% of the theoretical one. This indicates that some organic amine cations still remain in the

DOI: 10.1021/jacs.8b07457
J. Am. Chem. Soc. 2018, 140, 11133–11140

exchanged products, which is verified by IR spectroscopy (IR data analysis in SI).

The q_m^U values of FJSM-GAS-1 (196 mg/g) and FJSM-GAS-2 (144 mg/g) greatly exceed those of commercial resin products such as ARSEN-X^{np} Purolite resin (q_m^U = 47 mg/g),[21] strong base AMBERSEP 920U Cl resin (q_m^U = 50 mg/g),[22] and Tulsion CH-96 (q_m^U = 70 mg/g).[23] The q_m^{Cs} of FJSM-GAS-1 (164 mg/g) is also higher than that of commercial AMP-PAN (q_m^{Cs} = 81 mg/g), which is currently marketed by UOP as IONSIV IE-910.[24] The q_m^{Sr} of FJSM-GAS-1 (80 mg/g) is more than 5 times that of commercial AMP-PAN (q_m^{Sr} = 15 mg/g).[24] It is also higher than FJSM-SnS (q_m^{Sr} = 65 mg/g)[9d] and comparable to KMS-1 (q_m^{Sr} = 77 mg/g) (Table S10).[9i]

The value of the b constants in eq 2 represents an indicator for affinity toward a specific ion. The constants b (L/mg) are 0.022 ± 0.027 for uranium of FJSM-GAS-1 and 0.020 ± 0.005 for that of FJSM-GAS-2. For FJSM-GAS-1 the b values are 0.0046 ± 0.0007 for cesium and 0.0079 ± 0.0008 for strontium. The higher b (L/mg) values for uranium than for cesium and strontium indicate that FJSM-GAS-1 and FJSM-GAS-2 have stronger affinity toward the $[UO_2]^{2+}$ ion than for Cs^+ and Sr^{2+} ions.

Kinetic Studies of $[UO_2]^{2+}$ Ion Exchange. To further understand the ion exchange abilities of FJSM-GAS-1 and FJSM-GAS-2, we explored $[UO_2]^{2+}$ ion removal properties. We investigated the effects of contact time of $[UO_2]^{2+}$ ions with FJSM-GAS-1 and FJSM-GAS-2 to determine both ion exchange rates and equilibrium times. From Figure 5a, the kinetic data for the $[UO_2]^{2+}$ ion exchange by FJSM-GAS-1 showed the concentrations of uranium steeply decreased with time and the amount of U removed was 94.9% within the first 5 min. Significantly, the concentrations of uranium dropped from 1348 ppb to 5.5 ppb after 29 h, which is below the acceptable limit of 30 ppb for uranium in potable water defined by the U.S. Environmental Protection Agency (EPA).[25] The data for the $[UO_2]^{2+}$ ion exchange by FJSM-GAS-2 showed 86.9% removal within the first 5 min and 93.8% after the first 15 min. Thus, FJSM-GAS-1 and FJSM-GAS-2 display rapid kinetics with an equilibrium time of approximately 5 and 15 min, respectively. The rapid ion exchange kinetics derive from the layered nature of the structures and Lewis basic nature of sulfide frameworks. The equilibrium time of FJSM-GAS-2 is more than that of FJSM-GAS-1, which reflects the larger size of the diethylamine leading to slow escape from the structure.

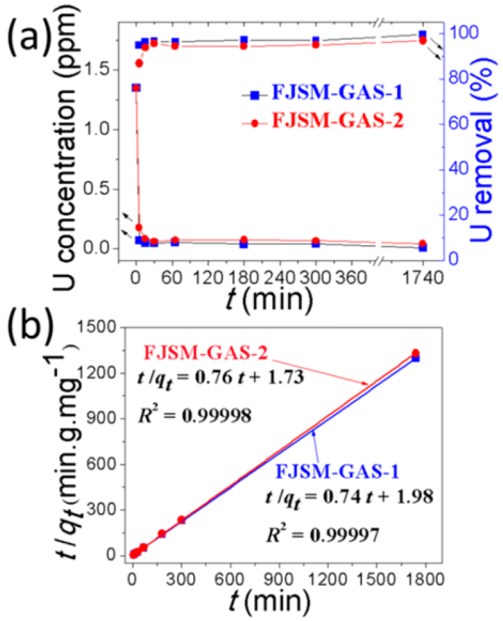

Figure 5. (a) Kinetics of $[UO_2]^{2+}$ ion exchange of FJSM-GAS-1 and FJSM-GAS-2 plotted as the U concentration (ppm) and the relative amount of U removed (%) vs the time t (min), respectively. (b) Plot of t/q_t vs t of the kinetics data of FJSM-GAS-1 and FJSM-GAS-2, which are well fitted with the pseudo-second-order kinetic model.

The kinetic data were further analyzed with pseudo-second-order kinetics, which presume that chemical adsorption is the rate-determining step.[26] It is expressed by eq 3. Here, q_t and q_e are the mass of a metal ion adsorbed per unit weight of adsorbent (mg·g^{-1}) at time t and at equilibrium, respectively. k_2 is the pseudo-second-order rate constant of the kinetic model (g·mg^{-1}·min^{-1}). q_e and k_2 can be calculated with the slope and intercept of the linear plot of t/q_t vs t of the kinetics data.

$$\frac{t}{q_t} = \frac{1}{k_2 q_e^2} + \frac{t}{q_e} \tag{3}$$

It is interesting that the plots of t/q_t vs t of the kinetics data for both compounds exhibit perfect linear relations (Figure 5b), which indicates both data can be well fitted with the pseudo-second-order kinetic model with high correlation coefficients R^2 (>0.99). The fitting results of the pseudo-second-order kinetic model are shown in Table S5. As we know, the pseudo-second-order kinetic model assumes that the rate-limiting step is chemical adsorption.[26] This further demonstrates that the U removal by both compounds involves chemical adsorption.

pH-Dependent $[UO_2]^{2+}$ Ion Exchange. Generally, nuclear waste solutions are very corrosive depending on the pH. So we conducted pH-dependent $[UO_2]^{2+}$ ion exchange experiments with FJSM-GAS-1 and FJSM-GAS-2. The distribution coefficient K_d is a measurement of affinity and selectivity and calculated with eq 4. The ion exchange efficiency, referred to as the relative amount of U removed (R), is described by eq 5. Here, C_f is the ending concentration of the ions.

$$K_d = \frac{V}{m}\frac{(C_0 - C_f)}{C_f} \tag{4}$$

$$R = \frac{(C_0 - C_f)}{C_0} \times 100\% \tag{5}$$

$[UO_2]^{2+}$ ion exchange experiments by FJSM-GAS-1 and FJSM-GAS-2 with a uranium concentration from 1468 to 2436 ppb were performed in the pH range of 2.9−10.5. Generally, a material with a K_d value more than 10^4 mL/g is viewed as an excellent adsorbent. At a pH of ∼5.1, it is noteworthy that the K_d^U values of FJSM-GAS-1 and FJSM-GAS-2 could rise to 2.47 × 10^4 and 5.12 × 10^4 mL/g, respectively (Figure 6a, Tables S6 and S7). As shown in Figure 6a, both compounds can remove uranium in the pH range of 2.9−10.5. The PXRD patterns of the $[UO_2]^{2+}$-exchanged products of FJSM-GAS-1 and FJSM-GAS-2 matched well with those of the pristine compounds, indicating that both compounds retained the parent frameworks in the ion exchange processes even at various pH values (Figure 6b and c). In fact, many oxidic ion exchangers are active only in a relatively narrow pH range,[5b] whereas the soft

DOI: 10.1021/jacs.8b07457
J. Am. Chem. Soc. 2018, 140, 11133−11140

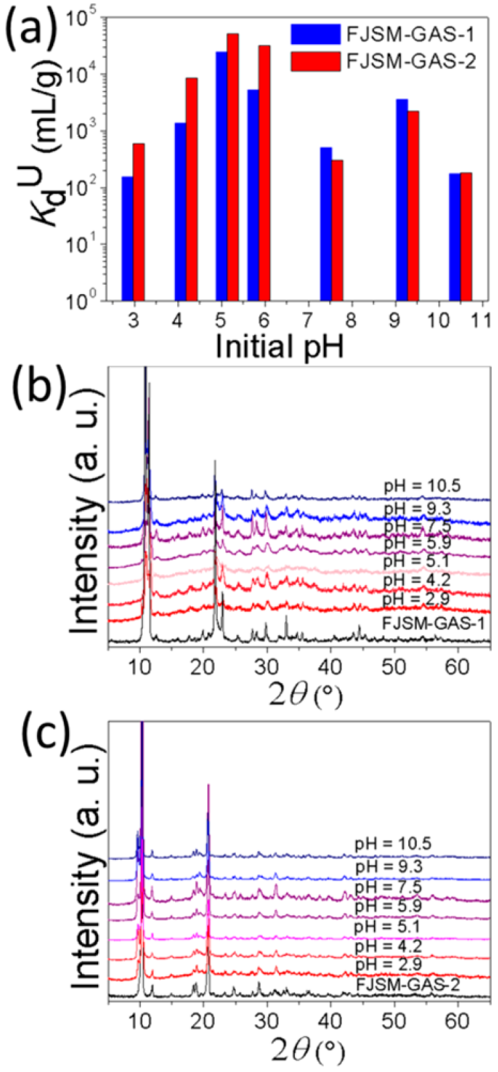

Figure 6. (a) Distribution coefficient K_d^U values of FJSM-GAS-1 and FJSM-GAS-2 at various initial pH values (C_0 in the range of 1468–2436 ppb for U, V:m = 1000 mL/g, at room temperature). PXRD patterns of products before and after $[UO_2]^{2+}$ ion exchange with various pH values for FJSM-GAS-1 (b) and FJSM-GAS-2 (c).

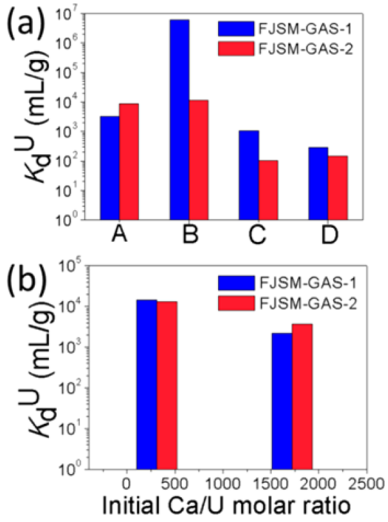

Figure 7. (a) Distribution coefficient K_d^U values (y-axis) of FJSM-GAS-1 and FJSM-GAS-2 in the different conditions (x-axis) in the presence of excess Na^+ or HCO_3^- (A: 0.3 M NaCl + 2.91 ppm U; B: 0.3 M $NaNO_3$ + 2.96 ppm U; C: 145 ppm of HCO_3^- + 2.58 ppb U; D: 0.3 M NaCl + 145 ppm of HCO_3^- + 3.34 ppb U). (b) Distribution coefficient K_d^U values of FJSM-GAS-1 and FJSM-GAS-2 under different Ca/U molar ratios.

Lewis basic S^{2-} sites of the title compounds have high affinity for $[UO_2]^{2+}$ over a wide pH active range (Table S10).

Effect of Na^+, Ca^{2+}, and HCO_3^- on $[UO_2]^{2+}$ Ion Exchange. High concentrations of nonradioactive alkali or alkaline earth metal ions such as Na^+ and Ca^{2+} and HCO_3^- anions are present in industrial waste and related solutions. These additional ions generally have a detrimental impact on the selective $[UO_2]^{2+}$ ion exchange. Therefore, we investigated $[UO_2]^{2+}$ ion exchange of FJSM-GAS-1 and FJSM-GAS-2 in the presence of a large excess of Na^+, Ca^{2+}, and HCO_3^-. Notably, K_d^U values could achieve 6.06×10^6 mL/g (FJSM-GAS-1) and 1.16×10^4 (FJSM-GAS-2) in a competitive exchange experiment containing 0.3 M $NaNO_3$ and 2.96 ppm U, respectively (Figure 7a, Table S8). To our knowledge, the K_d^U of 6.06×10^6 mL/g for FJSM-GAS-1 is the highest value among reported U adsorbents (Table S10).[9a,10a,b,27] Moreover, the initial U concentration of 2.96 ppm was reduced to the residual U concentration of 4.88 ppb, which is well below the acceptable level of 30 ppb. This represents 99.8% of U removal as well as strong affinity and very high selectivity for $[UO_2]^{2+}$ by FJSM-GAS-1 against Na^+.

As mentioned in the Introduction, trace concentrations of uranium (about 3.3 ppb) exist in the ocean.[3] Hence, we also examined the $[UO_2]^{2+}$ ion exchange performance of FJSM-GAS-1 and FJSM-GAS-2 toward trace uranium using simulated seawater. We observed that even in the presence of 145 ppm of HCO_3^- anions, FJSM-GAS-1 and FJSM-GAS-2 can capture U and reduced the U concentrations from 2.58 ppb to 0.41 ppb (FJSM-GAS-1) and 0.42 ppb (FJSM-GAS-2) (Figure 7a, Table S8), respectively. In the conditions of simulated seawater containing 0.3 M NaCl and 145 ppm of HCO_3^- with 3.34 ppb U, the ion-exchange efficiency R values of FJSM-GAS-1 and FJSM-GAS-2 could still reach 59.2% and 42.9%, respectively (Figure 7a, Table S8).

We also investigated the effect of Ca^{2+} ions on $[UO_2]^{2+}$ ion exchange, which usually act as strong competitors for $[UO_2]^{2+}$ capture in many absorbents. The results indicate that the K_d^U values of FJSM-GAS-1 and FJSM-GAS-2 can be more than 10^4 mL/g even with the addition of a more than 310 times higher concentration of Ca^{2+} ions. When the Ca:U molar ratio reached 1.72×10^3, K_d^U values of both compounds still achieved the level of 10^3 mL/g (Figure 7b, Table S9). Clearly, despite the presence of excess Na^+, Ca^{2+}, and HCO_3^-, FJSM-GAS-1 and FJSM-GAS-2 retain strong preference and high selectivity for $[UO_2]^{2+}$ ions.

Elution. The $[UO_2]^{2+}$-laden products of FJSM-GAS-1 and FJSM-GAS-2 could be eluted using a high concentration of KCl solution (0.2 M), a method found to be successful in our previous research.[10a,14] It is interesting that EDS analyses of the solids after elution indicate that the adsorbed $[UO_2]^{2+}$ ions were completely removed and replaced by K^+ ions (Figures S11 and S12). Furthermore, the elemental distribution mapping of K for both materials displays a homogeneous distribution (Figure 8). Thus, uranyl-laden products for FJSM-GAS-1 and FJSM-GAS-2 could be conveniently eluted with the low-cost method, which further highlights the potential for

DOI: 10.1021/jacs.8b07457
J. Am. Chem. Soc. 2018, 140, 11133–11140

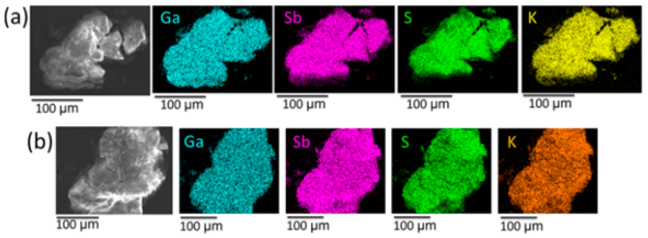

Figure 8. SEM images of the eluted products of $[UO_2]^{2+}$-exchanged FJSM-GAS-1 (a), $[UO_2]^{2+}$-exchanged FJSM-GAS-2 (b), and their elemental distribution maps of Ga, Sb, S, and K.

recycling of the title compounds in the capture of uranium from nuclear waste.

Organic Ammonium Cations and Ion Exchange Mechanism. Thus, far, several chalcogenidometalates containing protonated organic amine cations have exhibitied excellent ion exchange properties. For example, $[CH_3NH_3]^+$, $[Me_2NH_2]^+$, $[Me_3NH]^+$, and $DPAH^+$ (DPA = dipropylamine) can be easily exchanged by $[UO_2]^{2+}$, Cs^+, Sr^{2+} ions, etc. Therefore, monoamines can easily escape from the chalcogenide structures.[9c,d,10a,15,28] Even the bulky TAEA (tris(2-aminoethyl)ammonium) ions have been observed to ion exchange with Cs^+ ions via a stepwise ion exchange strategy.[29] In this work, we clearly demonstrated that the larger $[Et_2NH_2]^+$ could also be exchanged with $[UO_2]^{2+}$. Clearly, however, the cation size seems to matter, as FJSM-GAS-1 showed more rapid ion exchange kinetics and higher ion exchange capacities for uranium than FJSM-GAS-2, consistent with its smaller $[Me_2NH_2]^+$ cation. Obviously, the type, shape, and size of protonated organic amine cations in chalcogenido ion exchangers are important factors impacting ion exchange performance.[8]

CONCLUDING REMARKS

In conclusion, two radiation-resistant layered gallium thioantimonates with $[Me_2NH_2]^+$ and $[Et_2NH_2]^+$ cations have been found to exhibit excellent ion exchange performance for removing $[UO_2]^{2+}$, Cs^+, and Sr^{2+} ions. FJSM-GAS-1 is able to remove most of the low-concentration uranium even in the presence of a large excess of Na^+ ions with the residual U concentration of 4.88 ppb, which is below the acceptable level of 30 ppb for uranium in potable water defined by the EPA. The advantages of the title metal sulfide compounds as scavengers for radionuclides include (i) facile syntheses; (ii) excellent β and γ radiation resistance; (iii) high ion exchange capacities for $[UO_2]^{2+}$ ions; (iv) rapid kinetics; (v) wide pH active range for $[UO_2]^{2+}$ exchange; (vi) excellent selectivity for $[UO_2]^{2+}$ ions with high K_d values; and (v) convenient and low-cost elution method. Our findings validate previous reports[10a,c] that point to the uranium atom in the uranyl ion being not as hard a Lewis acid as it first might appear (given its 6+ formal oxidation state).[30] The hardness of the U^{6+} center is markedly mitigated by the two double bonds to the two oxygen atoms in the $[UO_2]^{2+}$ ion. This work further highlights the value and great potential of metal chalcogenides (especially sulfides) as radioactive ion exchangers in the field of environmental remediation.

ASSOCIATED CONTENT

Supporting Information

The Supporting Information is available free of charge on the ACS Publications website at DOI: 10.1021/jacs.8b07457.

Crystallographic data for FJSM-GAS-1 and FJSM-GAS-2; EDS analysis results and SEM images of pristine crystals and ion-exchanged products; PXRD patterns; IR spectra; XPS; ion exchange data for kinetic, pH-dependent experiments, the presence of excessive Na^+, Ca^{2+}, or HCO_3^-; EDS and PXRD analysis of eluted products (PDF)

X-ray crystallographic file for FJSM-GAS-1 (CIF)

X-ray crystallographic file for FJSM-GAS-2 (CIF)

AUTHOR INFORMATION

Corresponding Authors

*xyhuang@fjirsm.ac.cn

*m-kanatzidis@northwestern.edu

ORCID

Mei-Ling Feng: 0000-0003-2524-0994

Xiao-Ying Huang: 0000-0002-3514-216X

Mercouri G. Kanatzidis: 0000-0003-2037-4168

Notes

The authors declare no competing financial interest.

ACKNOWLEDGMENTS

We thank the National Science Foundations of China (Nos. 21771183, 21521061, and 21373223), the 973 programs (No. 2014CB845603), and Chunmiao project of Haixi Institute of Chinese Academy of Sciences (CMZX-2014-001). The work at Northwestern University was supported by the National Science Foundation (DMR-1708254). We also thank Prof. Shu-Ao Wang and Dr. Yan-Long Wang from School for Radiological and Interdisciplinary Sciences (RAD-X), Soochow University, China, for the radiation resistance experiments.

REFERENCES

(1) (a) Rivasseau, C.; Farhi, E.; Atteia, A.; Coute, A.; Gromova, M.; Saint Cyr, D. D.; Boisson, A. M.; Feret, A. S.; Compagnon, E.; Bligny, R. *Energy Environ. Sci.* **2013**, *6*, 1230−1239. (b) Boice, J. D., Jr. *J. Radiol. Prot.* **2012**, *32*, N33−N40. (c) Yoshida, N.; Kanda, J. *Science* **2012**, *336*, 1115−1116.

(2) Craft, E. S.; Abu-Qare, A. W.; Flaherty, M. M.; Garofolo, M. C.; Rincavage, H. L.; Abou-Donia, M. B. *J. Toxicol. Environ. Health, Part B* **2004**, *7*, 297−317.

(3) (a) Kim, J.; Tsouris, C.; Mayes, R. T.; Oyola, Y.; Saito, T.; Janke, C. J.; Dai, S.; Schneider, E.; Sachde, D. *Sep. Sci. Technol.* **2013**, *48*, 367−387. (b) Davies, R. V.; Kennedy, J.; Mcilroy, R. W.; Spence, R.; Hill, K. M. *Nature* **1964**, *203*, 1110−1115.

(4) Romanovskiy, V. N.; Smirnov, I. V.; Babain, V. A.; Todd, T. A.; Herbst, R. S.; Law, J. D.; Brewer, K. N. *Solvent Extr. Ion Exch.* **2001**, *19*, 1−21.

(5) (a) Manos, M. J.; Kanatzidis, M. G. *Chem. Sci.* **2016**, *7*, 4804−4824. (b) Rahman, R. O. A.; Ibrahium, H. A.; Hung, Y. T. *Water* **2011**, *3*, 551−565. (c) Jang, J. H.; Dempsey, B. A.; Burgos, W. D. *Environ. Sci. Technol.* **2007**, *41*, 4305−4310. (d) Bai, Z. Q.; Yuan, L. Y.; Zhu, L.; Liu, Z. R.; Chu, S. Q.; Zheng, L. R.; Zhang, J.; Chai, Z. F.; Shi, W. Q. *J. Mater. Chem. A* **2015**, *3*, 525−534. (e) Liu, W.; Dai, X.; Bai, Z.; Wang, Y.; Yang, Z.; Zhang, L.; Xu, L.; Chen, L.; Li, Y.; Gui, D.; Juan, D.; Wang, J.; Zhou, R.; Chai, Z.; Wang, S. *Environ. Sci. Technol.* **2017**, *51*, 3911−3921. (f) Al-Hobaib, A. S.; Al-Suhybani, A. A. *J. Radioanal. Nucl. Chem.* **2014**, *299*, 559−567. (g) Cao, Q.; Huang,

DOI: 10.1021/jacs.8b07457
J. Am. Chem. Soc. 2018, 140, 11133−11140

F.; Zhuang, Z.; Lin, Z. *Nanoscale* **2012**, *4*, 2423−2430. (h) Yang, W. T.; Bai, Z. Q.; Shi, W. Q.; Yuan, L. Y.; Tian, T.; Chai, Z. F.; Wang, H.; Sun, Z. M. *Chem. Commun.* **2013**, *49*, 10415−10417. (i) Riley, B. J.; Chun, J.; Um, W.; Lepry, W. C.; Matyas, J.; Olszta, M. J.; Li, X. H.; Polychronopoulou, K.; Kanatzidis, M. G. *Environ. Sci. Technol.* **2013**, *47*, 7540−7547. (j) Semiao, A. J. C.; Rossiter, H. M. A.; Schafer, A. I. *J. Membr. Sci.* **2010**, *348*, 174−180. (k) Riley, B. J.; Pierce, D. A.; Chun, J.; Matyas, J.; Lepry, W. C.; Garn, T. G.; Law, J. D.; Kanatzidis, M. G. *Environ. Sci. Technol.* **2014**, *48*, 5832−5839. (l) Wang, Y.; Liu, Z.; Li, Y.; Bai, Z.; Liu, W.; Wang, Y.; Xu, X.; Xiao, C.; Sheng, D.; Juan, D.; Su, J.; Chai, Z.; Albrecht-Schmitt, T. E.; Wang, S. *J. Am. Chem. Soc.* **2015**, *137*, 6144−6147. (m) Li, J.; Wang, X. X.; Zhao, G. X.; Chen, C. L.; Chai, Z. F.; Alsaedi, A.; Hayatf, T.; Wang, X. K. *Chem. Soc. Rev.* **2018**, *47*, 2322−2356.

(6) (a) Behrens, E. A.; Sylvester, P.; Clearfield, A. *Environ. Sci. Technol.* **1998**, *32*, 101−107. (b) Lehto, J.; Clearfield, A. *J. Radioanal. Nucl. Chem.* **1987**, *118*, 1−13.

(7) McKinley, J. P.; Zachara, J. M.; Smith, S. C.; Turner, G. D. *Clays Clay Miner.* **1995**, *43*, 586−598.

(8) Feng, M. L.; Wang, K. Y.; Huang, X. Y. *Chem. Rec.* **2016**, *16*, 582−600.

(9) (a) Sarma, D.; Malliakas, C. D.; Subrahmanyam, K. S.; Islama, S. M.; Kanatzidis, M. G. *Chem. Sci.* **2016**, *7*, 1121−1132. (b) Sarma, D.; Islam, S. M.; Subrahmanyam, K. S.; Kanatzidis, M. G. *J. Mater. Chem. A* **2016**, *4*, 16597−16605. (c) Zhang, B.; Feng, M. L.; Cui, H. H.; Du, C. F.; Qi, X. H.; Shen, N. N.; Huang, X. Y. *Inorg. Chem.* **2015**, *54*, 8474−8481. (d) Qi, X. H.; Du, K. Z.; Feng, M. L.; Li, J. R.; Du, C. F.; Zhang, B.; Huang, X. Y. *J. Mater. Chem. A* **2015**, *3*, 5665−5673. (e) Ding, N.; Kanatzidis, M. G. *Nat. Chem.* **2010**, *2*, 187−191. (f) Manos, M. J.; Petkov, V. G.; Kanatzidis, M. G. *Adv. Funct. Mater.* **2009**, *19*, 1087−1092. (g) Manos, M. J.; Kanatzidis, M. G. *Chem. - Eur. J.* **2009**, *15*, 4779−4784. (h) Mertz, J. L.; Fard, Z. H.; Malliakas, C. D.; Manos, M. J.; Kanatzidis, M. G. *Chem. Mater.* **2013**, *25*, 2116−2127. (i) Manos, M. J.; Ding, N.; Kanatzidis, M. G. *Proc. Natl. Acad. Sci. U. S. A.* **2008**, *105*, 3696−3699. (j) Feng, M. L.; Kong, D. N.; Xie, Z. L.; Huang, X. Y. *Angew. Chem., Int. Ed.* **2008**, *47*, 8623−8626. (k) Kanatzidis, M. G.; Manos, M. J. *J. Am. Chem. Soc.* **2009**, *131*, 6599−6607.

(10) (a) Feng, M. L.; Sarma, D.; Qi, X. H.; Du, K. Z.; Huang, X. Y.; Kanatzidis, M. G. *J. Am. Chem. Soc.* **2016**, *138*, 12578−12585. (b) Ma, S. L.; Huang, L.; Ma, L. J.; Shim, Y.; Islam, S. M.; Wang, P. L.; Zhao, L. D.; Wang, S. C.; Sun, G. B.; Yang, X. J.; Kanatzidis, M. G. *J. Am. Chem. Soc.* **2015**, *137*, 3670−3677. (c) Manos, M. J.; Kanatzidis, M. G. *J. Am. Chem. Soc.* **2012**, *134*, 16441−16446.

(11) Xiao, C.; Hassanzadeh Fard, Z.; Sarma, D.; Song, T. B.; Xu, C.; Kanatzidis, M. G. *J. Am. Chem. Soc.* **2017**, *139*, 16494−16497.

(12) (a) Manos, M. J.; Chrissafis, K.; Kanatzidis, M. G. *J. Am. Chem. Soc.* **2006**, *128*, 8875−8883. (b) Manos, M. J.; Iyer, R. G.; Quarez, E.; Liao, J. H.; Kanatzidis, M. G. *Angew. Chem., Int. Ed.* **2005**, *44*, 3552−3555.

(13) Ding, N.; Kanatzidis, M. G. *Angew. Chem., Int. Ed.* **2006**, *45*, 1397−1401.

(14) Qi, X. H.; Du, K. Z.; Feng, M. L.; Gao, Y. J.; Huang, X. Y.; Kanatzidis, M. G. *J. Am. Chem. Soc.* **2017**, *139*, 4314−4317.

(15) Li, J. R.; Huang, X. Y. *Dalton Trans* **2011**, *40*, 4387−4390.

(16) Wang, K. Y.; Feng, M. L.; Li, J. R.; Huang, X. Y. *J. Mater. Chem. A* **2013**, *1*, 1709−1715.

(17) Sheldrick, G. M. *Acta Crystallogr., Sect. A: Found. Adv.* **2015**, *71*, 3−8.

(18) (a) Feng, M. L.; Xie, Z. L.; Huang, X. Y. *Inorg. Chem.* **2009**, *48*, 3904−3906. (b) Kong, D. N.; Feng, M. L.; Ye, D.; Huang, X. Y. *Chin. J. Struct. Chem.* **2010**, *29*, 905−913. (c) Lin, Z. E.; Bu, X. H.; Feng, P. Y. *Microporous Mesoporous Mater.* **2010**, *132*, 328−334.

(19) Amayri, S.; Arnold, T.; Reich, T.; Foerstendorf, H.; Geipel, G.; Bernhard, G.; Massanek, A. *Environ. Sci. Technol.* **2004**, *38*, 6032−6036.

(20) (a) Abdel-Ghani, N. T.; Rawash, E. S. A.; El-Chaghaby, G. A. *Global J. Environ. Sci. Manage.* **2016**, *2*, 11−18. (b) Do, D. D. In *Adsorption Analysis: Equilibria and Kinetics*; Imperial College Press: London, 1998.

(21) Panturu, R. I.; Jinescu, G.; Panturu, E.; Filcenco-Olteanu, A.; Radu, D. A. *Rev. Chim.* **2011**, *62*, 814−817.

(22) Cheira, M. F.; El-Didamony, A. M.; Mahmoud, K. F.; Atia, B. M. *IOSR J. Appl. Chem.* **2014**, *7*, 32−40.

(23) Wnkatesan, K. A.; Shyamala, K. V.; Antony, M. P.; Srinivasan, T. G.; Rao, P. R. V. *J. Radioanal. Nucl. Chem.* **2008**, *275*, 563−570.

(24) Park, Y.; Lee, Y. C.; Shin, W. S.; Choi, S. *Chem. Eng. J.* **2010**, *162*, 685−695.

(25) Reimann, C.; Banks, D. *Sci. Total Environ.* **2004**, *332*, 13−21.

(26) Zhang, L.; Zhang, L.; Wu, T. H.; Jing, X. Y.; Li, R. M.; Liu, J. Y.; Liu, Q.; Wang, J. *RSC Adv.* **2015**, *5*, 53433−53440.

(27) Al-Attar, L.; Dyer, A. *J. Mater. Chem.* **2002**, *12*, 1381−1386.

(28) Ding, N.; Kanatzidis, M. G. *Chem. Mater.* **2007**, *19*, 3867−3869.

(29) Yang, H. J.; Luo, M.; Luo, L.; Wang, H. X.; Hu, D. D.; Lin, J.; Wang, X.; Wang, Y. L.; Wang, S.; Bu, X. H.; Feng, P. Y.; Wu, T. *Chem. Mater.* **2016**, *28*, 8774−8780.

(30) (a) Pearson, R. G. *J. Am. Chem. Soc.* **1963**, *85*, 3533−3539. (b) Parr, R. G.; Pearson, R. G. *J. Am. Chem. Soc.* **1983**, *105*, 7512−7516.

DOI: 10.1021/jacs.8b07457
J. Am. Chem. Soc. 2018, 140, 11133−11140